Mem. S.A.It. Suppl. Vol. 18, 53
© SAIt 2011

Memorie della
Supplementi

Pattern speed evolution and bar reformation

F. Combes

Laboratoire d'Etude du Rayonnement et de la Matiére (LERMA), Observatoire de Paris, Paris, France, e-mail: francoise.combes@obspm.fr

Abstract. Bars in spiral galaxies can weaken through gas inflow towards the center, and angular momentum transfer. Several bar episodes can follow one another in the life of the galaxy, if sufficient gas is accreted from the intergalactic medium to revive young disks. Pattern speeds of the successive bars are different, due to mass concentration, or increased velocity dispersion of the remaining stellar component. In the same time, the spiral galaxy evolves in morphological type. Numerical simulations are presented, trying to correlate type and bar pattern speeds.

Key words. galaxies: evolution – galaxy: ISM – galaxies: kinematics and dynamics – galaxies: star formation – galaxies: structure

1. Introduction

In the hierarchical scenario, most of the mass of galaxies is assembled through mergers of sub-units. Although this mechanism works pretty well for early-type galaxies and ellipticals, the interaction between galaxies is quite destructive for disks. To account for the high prevalence of thin disks in today's observations, another scenario has to be invoked in parallel, namely external gas accretion from filaments. This diffuse, progressive and smooth mass accretion is much less destructive, and helps to replenish galaxy disks in gas available for new star formation.

Gas accretion can reform cool and thin disks, which are then unstable to new spiral and bar patterns, in addition to star formation (Bournaud & Combes 2002). The relative role of gas accretion and mergers has recently been estimated in numerical simulations (Dekel et al 2009). The detailed analysis of a cosmological simulation with gas and star formation shows that most of the starbursts are due to smooth flows, which exceed the merger source by about a factor 10. Inflow rates are sufficient to assemble galaxy masses (10–100 $M_{\odot}\,yr^{-1}$).

These considerable gas flows should have large consequences on the dynamics of galaxy disks. In particular, they should accelerate the succession of patterns in the disk. The role of gas on bars has been investigated for a long time now (e.g., Friedli & Benz 1993).

In these early simulations, there was no dark matter component. The non-axisymmetric patterns produced gravity torques and the exchange of angular momentum between gas and stars and from inner to outer parts. The expulsion of the angular momentum in the outer parts, allows the gas to flow towards the center. This was accompanied by the destruction of the bar and formation of a triaxial bulge.

Send offprint requests to: Françoise Combes

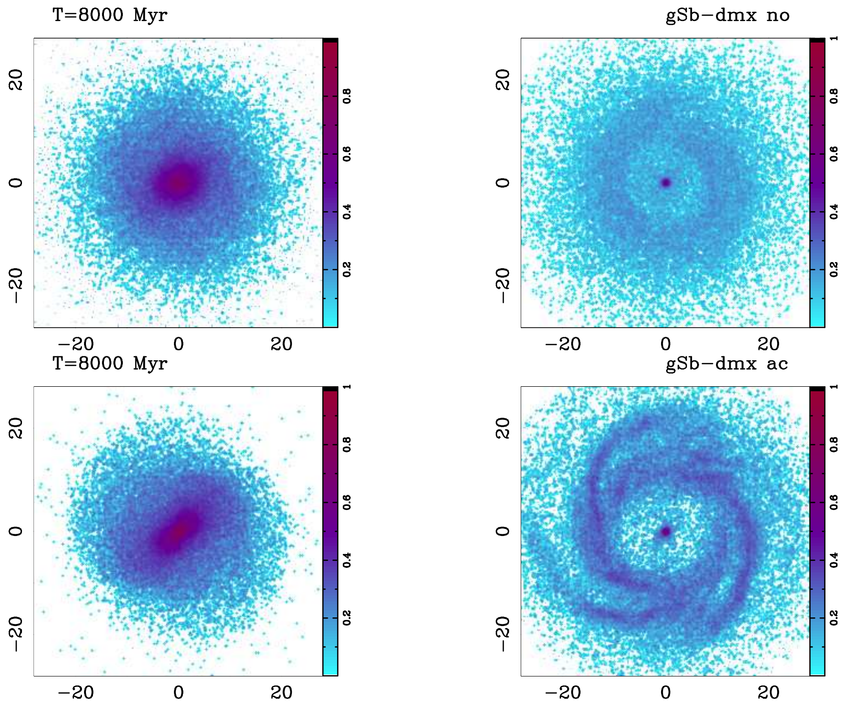

Fig. 1. Comparison between gSb galaxy models, without gas accretion (top) and with accretion (bottom). The gSb model is the maximum disk model, the gas accretion rate is 5 $M_\odot\,yr^{-1}$, and the snapshot corresponds to $T = 8$ Gyr. Note that a bar is maintained only in the case of gas accretion.

2. Bar formation and destruction

The mechanism invoked to account for the observed destruction of bars due to the gas inflow, was the implied central mass concentrations (CMC). When a massive CMC is added like a black hole in the center of a purely stellar disk, the effect is indeed to weaken and destroy bars (Norman et al. 1996). This is attributed to the chaos induced by the superposition of CMC and bar on the stellar orbits, as checked by the computation of surface of sections.

2.1. Bar destruction by gas

The effect of the gas inflow is not only to produce a central mass concentration. In fact, the gas is driven in by the bar torques, but reciprocally, the gas exerts the opposite torque on the stars. The angular momentum lost by the gas is taken up by the bar wave. Since the latter is a pattern with negative angular momentum (inside its corotation), this exchange of momentum weakens and destroys the bar. Simulations show that the gas infall of 1–2% of disk mass is enough to transform a bar in a lens (Friedli 1994; Berentzen et al. 1998; Bournaud et al. 2005).

2.2. Reformation of bars

If it is the gas inflow itself that destroys the bar, the advantage over the CMC mechanism is that it does not prevent a new bar to form. As soon as some new gas is accreted to replenish the disk, and makes it unstable again to bar formation, there could be a succession of patterns crossing the disk (see e.g., Fig. 1).

It works like a self-regulated cycle: the first step being the formation of a bar in a cold unstable disk, then the bar produces gas inflow, which weakens or destroys the bar. External gas accretion closes the loop. The gas enters

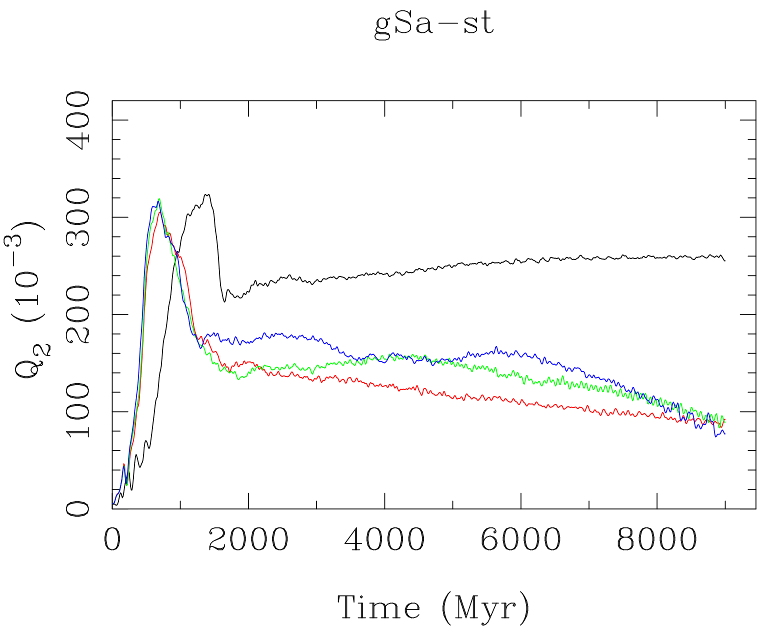

Fig. 2. Evolution of bar strength, measured as the ratio Q_2 of the maximal $m = 2$ tangential force to the radial force, measured at a radius of 3.3 kpc. The black curve corresponds to the purely stellar run, the red curve, to the spiral galaxy with initial gas, subject to star formation, but not replenished. These two curves are respectively the top and the bottom curves. The other curves corresponds to the models with gas accretion, 5 $M_\odot$ yr^{-1} for the green one, and 5 $M_\odot$ yr^{-1} for the blue one. The galaxy model is an early-type gSa. Note that the presence of gas triggers bar instability earlier than in the purely stellar run.

the disk by intermittence: first it is confined outside the OLR until the bar weakens, then it can replenish the disk, to make it unstable again to bar formation.

This is the mechanism when the dark matter component may be ignored, in the inner parts of giant galaxies. When a massive dark matter is taken into account in simulations, the angular momentum exchange is preferentially done with the DM particles, due to dynamical friction. Because of its low mass, the gas plays then a minor role in the angular momentum (AM) transfer, at least when the fraction of gas is lower than 8% (Berentzen et al. 2007).

However in dark matter (DM) dominated simulations, the bar is still weakened or destroyed more quickly in the presence of gas. This is interpreted in terms of the destruction by the gas of vertical resonances, and with the help of the CMC. To destroy the bar, the gas fraction must be higher in the presence of a massive halo.

The role of gas is complex since simulations reveal that it prevents peanut formation. The presence of gas implies more chaos in the orbits, which stop the effect of vertical resonance. However, the vertical peanut instability is a factor of bar weakening, in pure stellar disk. Since the bar is weakened more quickly in the presence of gas, the bar weakening mechanism must be different from the vertical buckling.

3. New simulations of bar reformation

To further investigate the relative role of gas and dark matter in the angular momentum transfer, and in the bar successive formation, weakening and re-formation, we have carried out a series of simulations, with different galaxy models, described in Table 1. Three

Table 1. Summary of the different models simulated (bulge, disk, halo and gas components are respectively described).

Model	M_b 10^{10} $M_\odot$	r_b kpc	M_d 10^{10} $M_\odot$	r_d kpc	M_h 10^{10} $M_\odot$	r_h kpc	M_{gas} 10^{10} $M_\odot$	r_{gas} kpc
gSa	4.6	2.0	6.9	4.0	11.5	10.0	1.3	5.0
gSb-st	1.1	1.0	4.6	5.0	17.2	12.0	0.9	6.0
gSb-dmx	2.2	1.0	9.2	5.0	11.4	12.0	0.9	6.0
gSb-nfw	1.1	1.0	4.6	5.0	17.2	12.0	0.9	6.0
gSd-st	0.0	–	5.7	6.0	17.2	15.0	1.7	7.0
gSd-dmx	0.0	–	11.4	6.0	11.4	15.0	1.7	7.0
gSd-nfw	0.0	–	5.7	6.0	17.2	15.0	1.7	7.0

Hubble types are considered, Sa, Sbc and Sd, and since they are giant spiral galaxies, they are noted gSa, gSb and gSd.

3.1. Prescription of the simulations

The simulations are fully self-consistent, with live dark haloes. They are using a 3D Particle-Mesh code, based on FFT, with a useful grid of 128^3 [the algorithm of James (1977) to suppress the Fourier images is used]. The gas is represented by sticky particles, and a total of 240,000 particles is used. Similar simulations with TREE-SPH have also been run (e.g., Di Matteo et al. 2007).

The star formation is assumed to follow a Schmidt law, with exponent $n = 1.4$, and a density threshold. It is calibrated for a gas consumption time-scale of 5 Gyr. We do not assume instantaneous recycling, but take into account a continuous mass loss, across Gyrs (Jungwiert et al. 2001). The mass loss by stars is distributed through gas on neighbouring particles, with a velocity dispersion, to schematize the feedback energy.

When external gas accretion is considered, the gas is deposited at the inner border of the disk, over 4 kpc. At this radius, the gas is assumed to have already settled in the plane, with circular velocity. To cope with large mass variations of the gas component, the number of gas particles is kept constant, but the individual particle mass is variable. The same is assumed for the 'star' particles, which can be newly born, or lose mass.

The mass and characteristic radii of all components in the seven initial conditions, are displayed in Table 1. The standard model has a disk dominated by dark matter, but with a core. An NFW model, with a cusp and a central concentration of $c = 8$ has been run, then a maximum disk model (dmx) with equal mass in baryons and DM within the optical disk. For each galaxy model, we have 4 runs: a control simulation with pure stellar disks, without gas, then a run with gas and star formation, and two other runs with gas accretion, either 5 $M_\odot$ yr^{-1}, or 10 $M_\odot$ yr^{-1}.

The rotation curves are fitted to the observed typical curves for these Hubble types. For these giant spiral galaxies, the total mass inside 35 kpc is 2.4×10^{11} $M_\odot$, with 75% DM and 25% baryons, for the standard model (and equality between baryons and DM for the dmx model). In the gas accretion runs, the final mass is 17% or 35% higher after 9 Gyr. Due to the varying bulge-to-disk mass ratio over the sequence, the precession rate $\Omega - \kappa/2$ sweeps a large range, so that the expected pattern speed of the bar patterns are expected to vary correspondingly.

The bar strength and pattern speed are computed from Fourier analysis of the potential, as in Combes & Sanders (1981)

$$Q_2 = F_\theta(m = 2)/F_r. \quad (1)$$

We take the maximum over the azimuth of Q_2, estimated at a radius of $R = 3.3$ kpc.

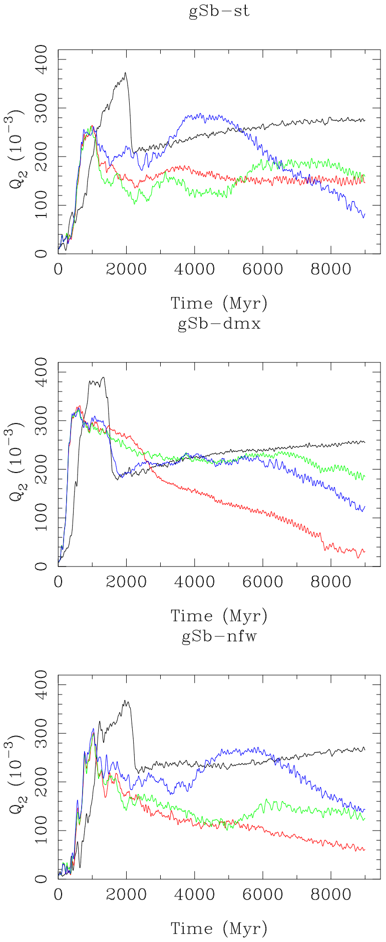

Fig. 3. Evolution of bar strength, as in Fig. 2 (black is the purely stellar run, red with gas but no accretion, green with 5 $M_\odot\,yr^{-1}$ accretion, and red 10 $M_\odot\,yr^{-1}$), for the 3 potential models of the gSb galaxy: standard, maximum disk, and cuspy NFW dark matter halo.

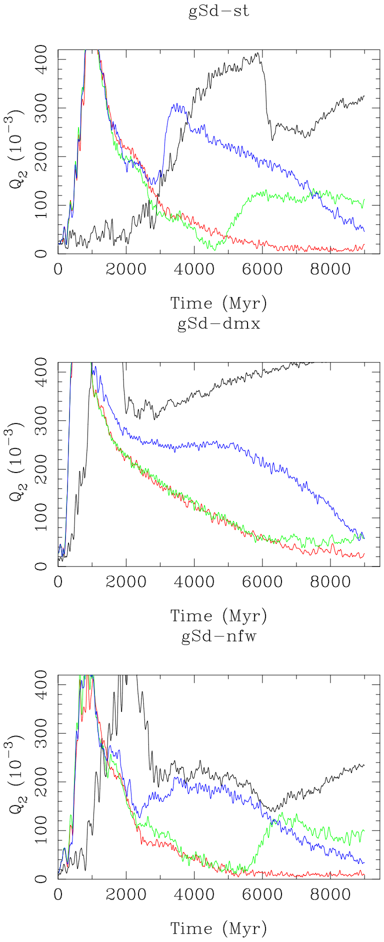

Fig. 4. Same as in Fig. 3, but for the gSd models.

3.2. Angular momentum transfer

When the galaxy disk is dominated by the mass of the dark matter halo, the main AM transfer is from baryons to the dark matter (Athanassoula 2002, 2003). In that sense, the DM halo can favor (instead of prevent) bar formation.

With light dark matter haloes, the bar is formed or weakened while AM is exchanged between the inner disk and the outer disk or gas. The exact process depends on the amount of dark matter inside the visible disk.

In addition, the pattern speed of the bar decreases due to dynamical friction against the dark matter particles (Debattista & Sellwood 2000). We observed the same phenomenon with our standard models, in the case of pure stellar disks. In the gSa model for instance, the pattern speed Ω_b begins at 50 km s^{-1} kpc^{-1}, and the bar slows down until around 10 km s^{-1} kpc^{-1} in the pure stellar run. With initial gas, and no accretion, the bar is quickly weakened, and there is then three times less

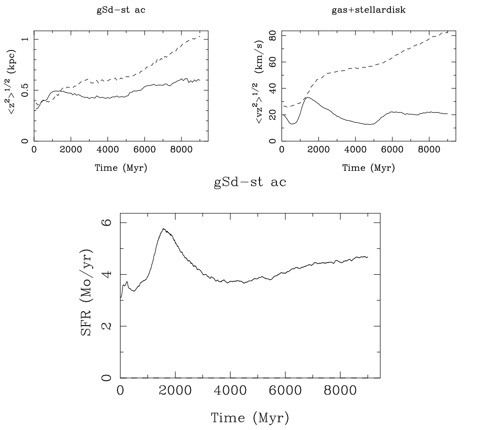

Fig. 5. Star formation rate versus time (bottom), average plane thickness (top left), and vertical velocity dispersion (top right), for the gSd standard model. The dashed lines correspond to the stellar component, and the full lines to the gas.

angular momentum transfer: Ω_b decreases less, from 50 to 25 km s^{-1} kpc^{-1}, in 9 Gyr.

3.3. Comparison of bar strengths

Fig. 2 compares the bar strength of several runs, in the case of the gSa galaxy model. When the disk is purely stellar, the bar is long lived (black curve), although it is suddenly weakened when the peanut resonance thickens the disk vertically. When the gas is included (and for this early-type galaxy, it is 5% of the total mass), then the bar is destroyed (red curve). Note that with gas, the bar instability occurs earlier than in the pure stellar case, since the disk is then cooler, and thus more unstable. With gas accretion (5 $M_\odot$ yr^{-1}), the bar remains at a higher level, even more with a double accretion rate (10 $M_\odot$ yr^{-1}), although the effect remains small. This might be due to the great stability conferred by the massive bulge.

The same features occur also in the case of the gSb model (Fig. 3), but now the gas accretion succeeds to reform a new bar, at the same level as the control run, with a purely stellar disk.

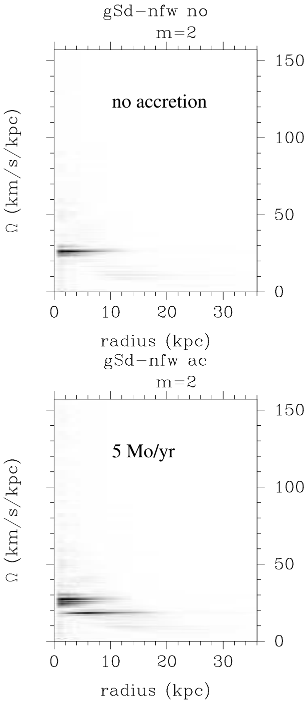

Fig. 6. Power spectrum displaying the pattern speed of the $m = 2$ Fourier component, over the whole simulation of the gSd model, version NFW potential, without accretion (top), and with accretion by 5 $M_\odot$ yr^{-1} (bottom). Without gas accretion, the bar is destroyed rapidly, and has no time to slow down, due to dynamical friction. The signature shows a single pattern speed. For the case with gas accretion, a new bar is formed, with a smaller pattern speed, and several values can be read. Note that the bar is more extended, when slower.

The case of the gSd model is more complex (Fig. 4). The instability of the disk is large, and dynamical feedback effects, due to gravitational heating, can produce unexpected behaviour. The dark matter halo stabilises the standard gSd model; the thin disk, in the absence of a bulge, is vertically unstable, and buckles even before forming a bar, which delays by 4 Gyr the bar formation. In presence of gas, the bar forms in less than 1 Gyr however. Second bar episodes are observed.

Fig. 5 shows how gas accretion can maintain the star formation rate at a nearly con-

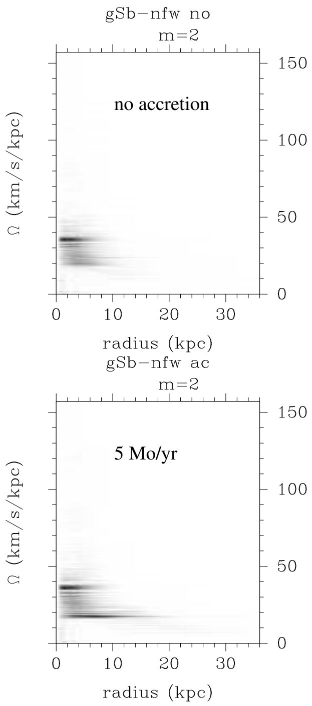

Fig. 7. Power spectrum displaying the pattern speed of the $m = 2$ Fourier component, over the whole simulation of the gSb model, version NFW potential, without accretion (top), and with accretion by 5 $M_\odot\,yr^{-1}$ (bottom). Note how thick is the spectrum, accumulating several bar patterns with slower and slower speeds. With gas accretion, a new, more extended, bar is formed, with a smaller pattern speed.

stant value, while it is exponentially decreasing without external gas accretion. The star formation and corresponding feedback progressively heats the stellar disk (visible both in vertical height of the disk and vertical velocity dispersion). The peanut formation heats also the stars, while the gas can cool down, and retrieve an approximately constant $z-$dispersion.

4. Pattern speeds

The normal bar evolution is often accompanied by a decrease of the pattern speed, and this phenomenon occurs even without dark matter halo and dynamical friction. This phenomenon was observed in models without DM halo, or with rigid haloes (Friedli & Benz 1993). Stellar orbits are more and more elongated during bar growth, and their precession rate decreases (e.g., Combes et al. 1990). This AM exchange with the outer disk is also accompanied by chaotic escape. More unstable stellar disks end up with a weaker bar.

Fig. 6 shows the power spectrum of the NFW-potential gSd model. The power spectrum is defined by the Fourier transform over time of the bar strength, at each radius

$$\mathrm{Power}(\omega, r) = \int Q_2(t, r) \exp(i\omega t) dt. \qquad (2)$$

In the case of no gas accretion, the bar is quickly destroyed, and the spectrum is clear and thin: only one bar at 28 $\mathrm{km\,s^{-1}\,kpc^{-1}}$ is seen. With gas accretion, a second bar is formed, but with lower pattern speed, 18 $\mathrm{km\,s^{-1}\,kpc^{-1}}$, and two features are seen in the power-spectrum. In the case of a bar only weakened, but not destroyed, and slowed down by dynamical friction, a thick spectrum is observed, as a tracer of the continuously decreasing pattern speed (cf. Fig. 7).

It is important to note that bars always end up near their corotation. When the bar is slowed down, its length increases correspondingly. Fig. 6 shows clearly how the slower bar is more extended in radius. It will then be quite difficult observationally to retrieve the history of the bar pattern speed evolution.

As a consequence of AM transfers, mass is redistributed in the disk, and the surface density reveals breaks in the radial profiles. Surface density breaks have been interpreted as the formation of successive bars by Debattista et al. (2006). These could be a stellar process (Pfenniger & Friedli 1991), or a gas process, with star formation threshold (Roškar et al. 2008).

5. Conclusions

Gas plays a fundamental role in spiral galaxies. Even when representing only 5–7% of the total mass inside 35 kpc, the presence of gas weakens or destroys the bar. It can weaken the peanut and change the bar pattern speed.

To account for the bar frequency observed today, it is essential to take into account gas accretion: it provides bar reformation, through disk replenishment. The amount of gas accretion required is justified and confirmed by cosmological simulations.

It is possible that mass assembly could be attributed to smooth accretion more than mergers: this will solve the problem of the high frequency of bars observed today, and also the existence of thin stellar disks, that mergers would over-heat.

Finally, pattern speeds have a tendency to decrease, first due to the elongation of orbits, and the heating of the disk, then bars are slowed down by dynamical friction against the dark halo. When bars are reformed, they occur with a lower pattern speed. This may constrain the amount of dark matter present within the optical disk.

Acknowledgements. I am grateful to E. M. Corsini and V. P. Debattista to invite me at such an exciting and friendly conference.

References

Athanassoula, E. 2002, ApJ, 569, L83
Athanassoula, E. 2003, MNRAS, 341, 1179
Berentzen, I., Heller, C. H., Shlosman, I., & Fricke, K. J. 1998, MNRAS, 300, 49
Berentzen, I., Shlosman, I., Martinez-Valpuesta, I., & Heller, C. 2007, ApJ, 666, 189
Bournaud, F., & Combes, F. 2002, A&A, 392, 83
Bournaud, F., Combes F., & Semelin, B. 2005, MNRAS, 364, L18
Combes, F., & Sanders, R. H. 1981, A&A, 96, 164
Combes, F., Debbasch, F., Friedli, D., & Pfenniger, D. 1990, A&A, 233, 82
Debattista, V. P., & Sellwood, J. 2000, ApJ, 543, 704
Debattista, V. P., Mayer, L., Carollo, C. M., et al. 2006, ApJ, 645, 209
Dekel, A., Birnboim, Y., Engel, G., et al. 2009, Nature, 457, 451
Di Matteo, P., Combes, F., Melchior, A-L., & Semelin, B. 2007, A&A, 468, 61
Friedli, D. 1994, in Mass-Transfer Induced Activity in Galaxies, ed. I. Shlosman (Cambridge Univ. Press, Cambridge), 268
Friedli, D., & Benz, W. 1993, A&A, 268, 65
James, R. A. 1977, J. Comput. Phys., 25, 71
Jungwiert, B., Combes, F., & Palous, J. 2001, A&A, 376, 85
Norman, C., Sellwood, J. A., & Hasan, H. 1996, ApJ, 462, 114
Pfenniger, D., & Friedli, D. 1991, A&A, 252, 75
Roškar, R., Debattista, V. P., Quinn, T. R., Stinson, G. S., & Wadsley, J. 2008, ApJ, 684, L79